SUPPLEMENTARY INFORMATION

The hemifusion structure induced by Influenza virus hemagglutinin is determined by physical properties of the target membranes

Petr Chlanda, Elena Mekhedov, Hang Waters, Cindi L. Schwartz, Elizabeth R. Fischer, Rolf J. Ryham, Fredric S. Cohen, Paul S. Blank and Joshua Zimmerberg

SUPPLEMENTARY RESULTS

Continuum analyses of hemifusion stalk expansion and rupture-insertion pathways in relationship to cholesterol concentration.

After calculating free energy as described in the main text, the distributional analyses were normalized with respect to the most probable diameter; the continuum energies are at their minima at this reference state, and were arbitrarily set to 0 kT. This allowed the numerical HD distributions to be compared in terms of relative energy, ΔE. We used the function exp(-ΔE/kT) of HD diameter to calculate PDFs by continuum simulation. The PDFs predicted by continuum theory are narrower and their tails shorter than the distributional PDFs derived from the experimental data (Fig. 4e). A plausible explanation for this discrepancy could be that the theoretically predicted sizes of HDs assumes a pathway where the distal monolayer areas are fixed, whereas the membrane surface area of the experimental VLP and liposomes vary between samples. Combinations of VLP and liposome areas that are energetically less costly would be experimentally represented more often. The continuum mechanics energies ignore this weighting, and should be somewhat larger than the energies calculated from the

distribution of HD diameters taken from the entire experimental population. Nevertheless, the theoretical prediction of HD stability and its expected diameter were in remarkable accord with the experimental results; in fact, the relative probabilities and minimal HD diameter from the continuum and distributional (experimental data) PDFs were the same (Fig. 4e). Both the hemifusion stalk expansion pathway and rupture-insertion pathway toward hemifusion possess HD diameters of miminal energy. But the mechanisms promoting or preventing growth are different for these two pathways.

In the hemifusion-stalk expansion pathway (Fig. 4e and Supplementary Fig. 8e, green curve), the HD is comprised of two monolayer leaflets, one from the viral envelope and the other from the liposome; the HD forms by the abutment between apposing distal monolayers. The composition of each of these monolayers was assumed to be uniform and the same as their respective monolayers outside the HD. In this pathway, HD widening is promoted by the match between membrane curvature of the proximal liposome/VLP monolayers (Supplementary Fig. 8a and 8b) and the negative spontaneous curvatures (40 mol % cholesterol, k_0 = -0.24 nm^{-1} in the liposome, k_0 = -0.13 nm^{-1} in the VLP). But HD widening requires that lipids from the distal monolayers move into the diaphragm, decreasing the overall area of the non-HD monolayers. Lipids from the proximal monolayers do not migrate into the HD and, as a result, further HD growth is prevented by compression of the proximal monolayers (K_A = 33 kT nm^{-2}).

For the rupture-insertion pathway (Fig. 4e and Supplementary Fig. 8e, blue and red curves), we assume that the diameter of the HD is equal to that of the binding area between the VLP with its complement of HA and the liposome. This assumption is consistent with the observation that the distributions of binding area are similar to HD

areas and that these HD interiors could contain HA. A Hookean binding potential with energy $\Delta G_0\pi(D/2+l_0)^2 A_0^{-1}$ was used to numerically enforce the condition that the proximal monolayers of the initially spherical liposome and VLP bilayers adhered to form a common surface of prescribed diameter D (Supplementary Fig. 8c and 8d). To obtain the adhesion energy, we used ΔG_0 = -11 kT (-6.4 kcal mol^{-1}) for the Gibbs energy for insertion of an HA fusion peptide into the liposome membrane [1] and A_0 = 91 nm^2 for the surface area per HA (~11 glycoproteins per 1000 nm^2). In this pathway, expansion of the initial HD is favored since the energy gained in binding is greater than the energy required to locally flatten the apposing proximal monolayers (Supplementary Fig. 8c). But beyond the minimal HD diameter, growth is prevented by the elastic energy required to support the increasingly deformed shapes (Supplementary Fig. 8d). In contrast to the hemifusion stalk expansion pathway, the energies of the rupture-insertion pathway are relatively insensitive to cholesterol composition since the curvatures of the bound proximal monolayers do not match any of the spontaneous curvatures (Fig. 4e and Supplementary Fig. 8e, red curve k_0 = -0.07 nm^{-1}, blue curve k_0 = -0.13 nm^{-1}).

We also used continuum analysis to investigate the effect of cholesterol concentration on the energy required to form an initial hemifusion-stalk. The reference energy E_0 of a spherical liposomes and VLP (prior to merger) varies with spontaneous curvature, and in turn varies with cholesterol concentration since k_0 becomes increasingly negative for increases in cholesterol concentration. Comparing the energy E of a stalk shape (HD diameter 6 nm) with the reference energy E_0, we find that the relative change in energy decreases with increases in cholesterol concentration, and becomes negative at approximately 31 mol % cholesterol (Fig. 4f, inset). For concentrations much less than 31

mol %, stalk formation requires a large amount of energy. Hence, for low concentrations an energetically more favorable trajectory would be taken, such as the rupture-insertion pathway. Conversely, for concentrations of cholesterol greater than 31 mol %, the stalk expansion pathway for hemifusion will be favored over the rupture-insertion pathway.

Lipidic junction and HD dependencies on M1 layer.

Experimentally, the appearance of lipidic junctions was independent of the M1 layer in G1S VLP (Supplementary Fig. 4a). Lipidic junction chord lengths and HD diameters both with and without a M1 layer were log-normally distributed with averages not significantly different (17±7 nm; n=24) and (21±14 nm; n=27), respectively (Supplementary Fig. 4b and 4c). WT chord lengths in the presence (19±4 nm; n=13) and absence (23±12 nm; n=11) of M1 layer were similar to those found for G1S. However, we found that the standard deviations of chord lengths were significantly different (Levene's test; $p = 3.8e^{-3}$) when comparing data with and without the M1 layer in both WT and G1S. Consistently, "Y" angles with and without M1 layer had significantly different averages 93±21°and 77±17° in G1S VLP ($p = 0.004$; Kolmogorov-Smirnov test) (Supplementary Fig. 4b and 4d).

In order to quantitatively evaluate the dependency of hemifusion energy on the M1 layer, we considered lipidic junctions where the leaflets of a liposome membrane are inserted into the viral membrane outer leaflet. For these calculations, both monolayers of the HD are comprised of viral envelope. (In the previous rupture-insertion calculations, distributions were inferred from binding energetics). The elastic constants were: k_0= -

0.13 nm^{-1}; K_C = 3 kT, K_θ= 3 kT nm^{-2}; K_A= 9 kT nm^{-2} in the liposomal bilayer and k_0 = 0.1 nm^{-1}; K_C = 10 kT, K_θ = 10 kT nm^{-2}; K_A = 30 kT nm^{-2} in the VLP-HD bilayers [2,3]. When inspecting the cET images, the matrix layer appears to constrain the VLP to a sphere; this was accounted for by integrating a penalty term $1/2K_M(\mathbf{d}\cdot\boldsymbol{\tau})^2$ with tangent vector $\boldsymbol{\tau}$ along the inner VLP monolayer; we set K_M = 2.0 kT nm^{-2} when the matrix layer was present, and K_M = 0.0 kT nm^{-2} when the matrix layer was absent. Liposomes merged to the VLP by lipid junctions were teardrop shaped (Supplementary Fig. 4 and 10); we included a repulsion potential with pressure at zero separation P_0 = 0.25 x 10^{-9} Pa and decay length λ = 0.37 nm [4] to prevent the apposing monolayers of the liposome neck from collapsing onto each other (Supplementary Fig. 10). The VLP-HD area is larger than the liposome area because the former includes the area of the HD. This was accounted for by constraining the liposome and VLP-HD inner monolayer areas to 29,000 nm^2 (radius 48 nm prior to merger) and 35,600 nm^2 (radius 53 nm prior to merger) respectively. This represents the size distributions when both particles have diameter roughly 100 nm.

Normalized free energy (ΔE) calculated by a standard Helfrich Hamiltonian (Materials and Methods) reproduced well the ΔE inferred from our distributional analysis for the above elastic parameters (Supplementary Fig. 4e, 4f). The theoretical probability distribution exp(-ΔE/kT) was fit well by a log-normal PDF/CDF (Supplementary Fig. 10d and 10e). Calculated minimal shapes for different HD diameters, with and without the matrix layer, are shown in Supplementary Fig. 10a-c. They are similar to the bilayer shapes in the cET images (Supplementary Fig. 4a). The interpretation of the theoretical energy curves (Supplementary Fig. 4e and 4f) is that for HD diameters greater than at the energy minimum, the neck of the liposomal bilayer is less pinched than for small HD

diameters and hence the splay energy of the liposome monotonically decreases. For diameters smaller than at the energy minimum, the inner walls of the narrow liposomal neck repel. Moving these walls apart (increasing HD diameter), relieves the inter-monolayer pressure (Supplementary Fig. 10a, inset), accounting for roughly one half of the drop in total energy. Widening of the HD allows the outer VLP-HD lipids of the "Y" to assume a less vertical alignment (Supplementary Fig. 10 and 10b, insets). This relaxes the liposomal tilt deformation and yields a further reduction in total energy. In the VLP bilayer, the overall splay energy decreases with HD diameter; the growth of HD splay is quadratic, but this growth is less steep than the decrease in the splay of the non-HD bilayer. Thus, the elastic force due to splay in both the liposome and VLP-HD favors widening of the HD. This overall decrease in splay energy is overcome by the considerable energy stored in tilt and stretching the "Y," which grows proportionally with HD circumference, and increases with the presence of the M1 layer. In summary, these findings suggest that the presence of the M1 layer constrains the size variance through modulation of membrane rigidity.

SUPPLEMENTARY FIGURES

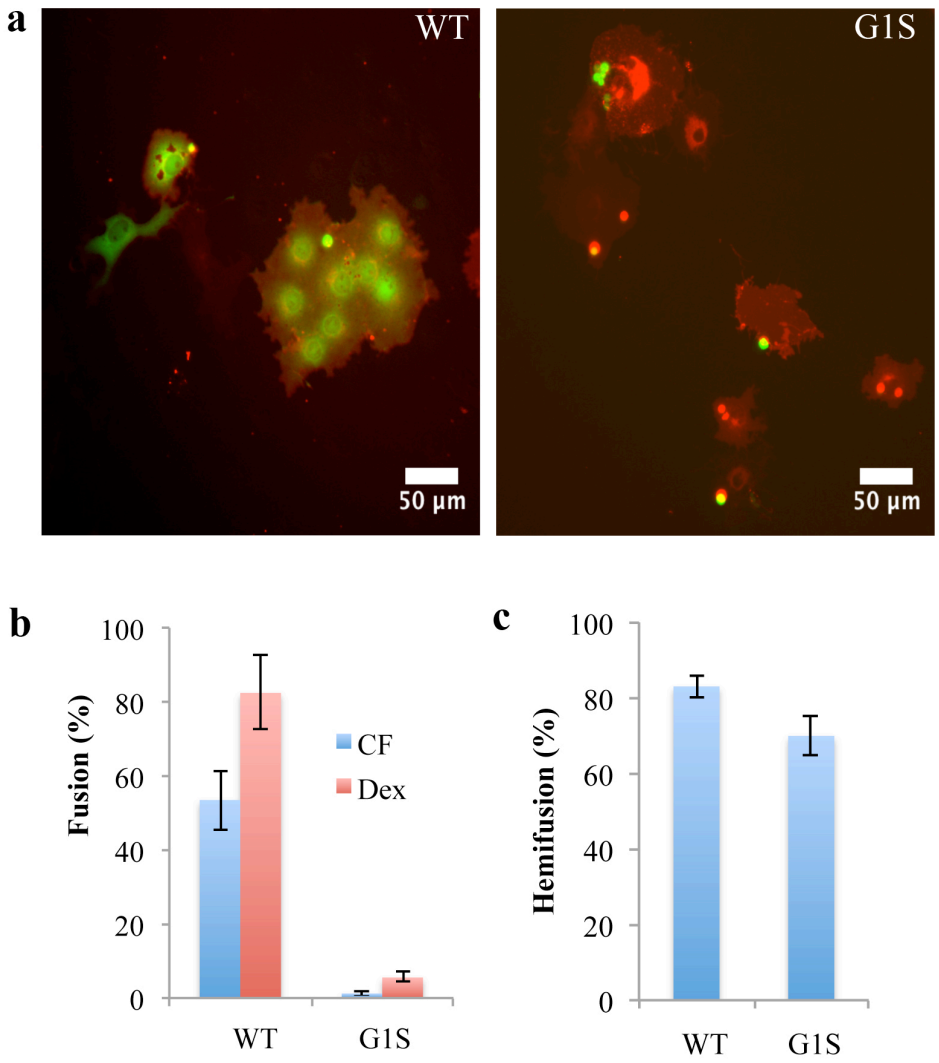

Supplementary Figure 1. Cell-red blood cell (RBC) fusion assay show that G1S mutation in HA fusion peptides mediates hemifusion but not full fusion. **a**, Set of representative fluorescent micrographs of pairs of RBC and transfected Cos7 cells stimulated to fuse. Cos7 cells were transfected 24 h prior fusion with either HA WT or G1S, incubated with RBC labeled with both PKH lipid dye mixing (red) and either with FITC-dextran (10 kDa) or carboxyfluorescein aqueous dyes (green). Fusion was triggered by exposure to citrate buffer with pH 4.9 for 2 min at 37°C, followed by 20 min at pH 7 prior to imaging and counting fusion phenotype outcomes. G1S HA was not able to

induce fusion pores that supported mixing of both carboxyfluorescein and 10 kDa FITC-dextran. **b**, Bar plot of counted fusion events of content mixing (green cells containing either carboxyfluorescein or 10 kDa FITC-dextran) normalized to lipid mixing events (red cells labeled with PKH) driven by HA WT and G1S. **c**, Bar plot of cells showing hemifusion mediated by either HA WT or G1S hemifusion mutant normalized to total number of cells. Bars represent a mean value of 3 independent experiments and error bars represent standard error of the mean.

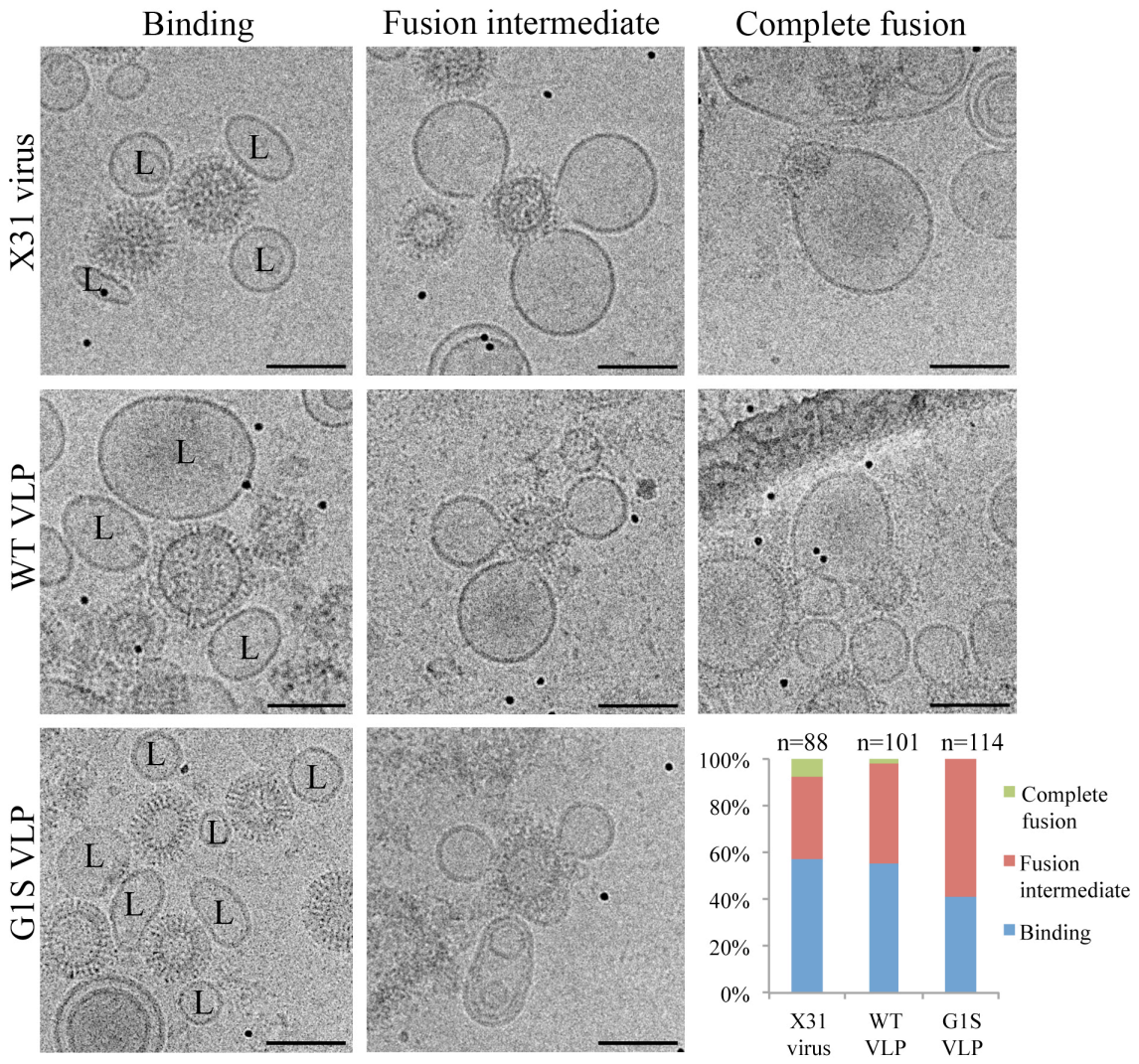

Supplementary Figure 2. Influenza VLP can carry mutated HA and shows similar response to low pH as influenza virus X31. cEM projections capturing liposome-influenza virus X31, -WT VLP or -G1S VLP clusters in a bound, fusion intermediate, or completely fused state. Influenza X31 virus and VLP were mixed with liposomes containing 16 mol % cholesterol and 5 mol % total gangliosides as the source for the influenza sialic acid receptor for 20 min at neutral pH and subjected to low pH for 2 min at 37°C. Three different stages of fusion: (i) binding, (ii) fusion intermediate and (iii) complete fusion are based on criteria (Materials and Methods: cEM of VLP and liposome fusion products and quantification). Bound liposomes are labeled with "L". Scale bars: 100 nm.

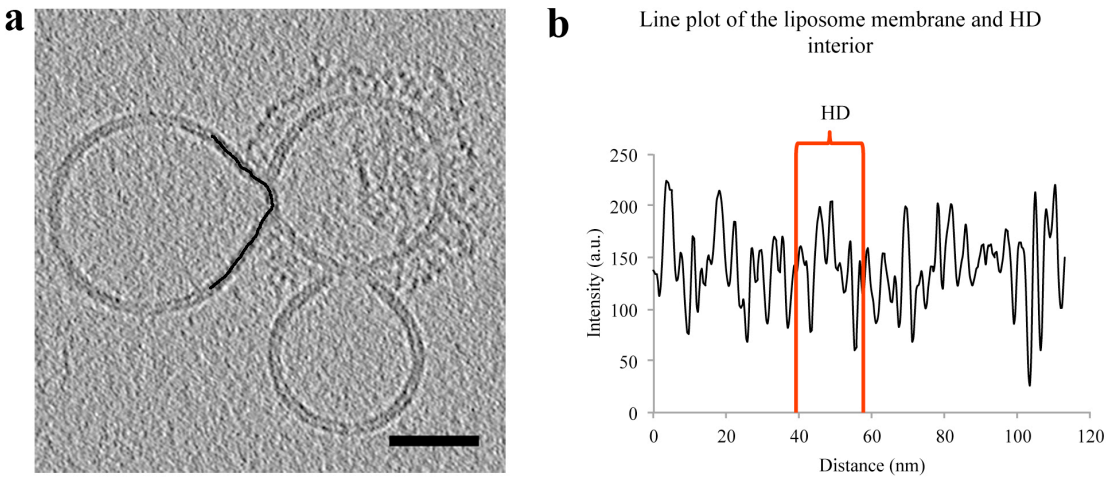

Supplementary Figure 3. "Y" junction and liposome membrane interior densities are similar. a, Same as in Fig. 2b. Scale bar: 50 nm. **b**, Line plot shows density (grey value) inside the liposome membrane and HD. Red vertical lines mark HD boundaries.

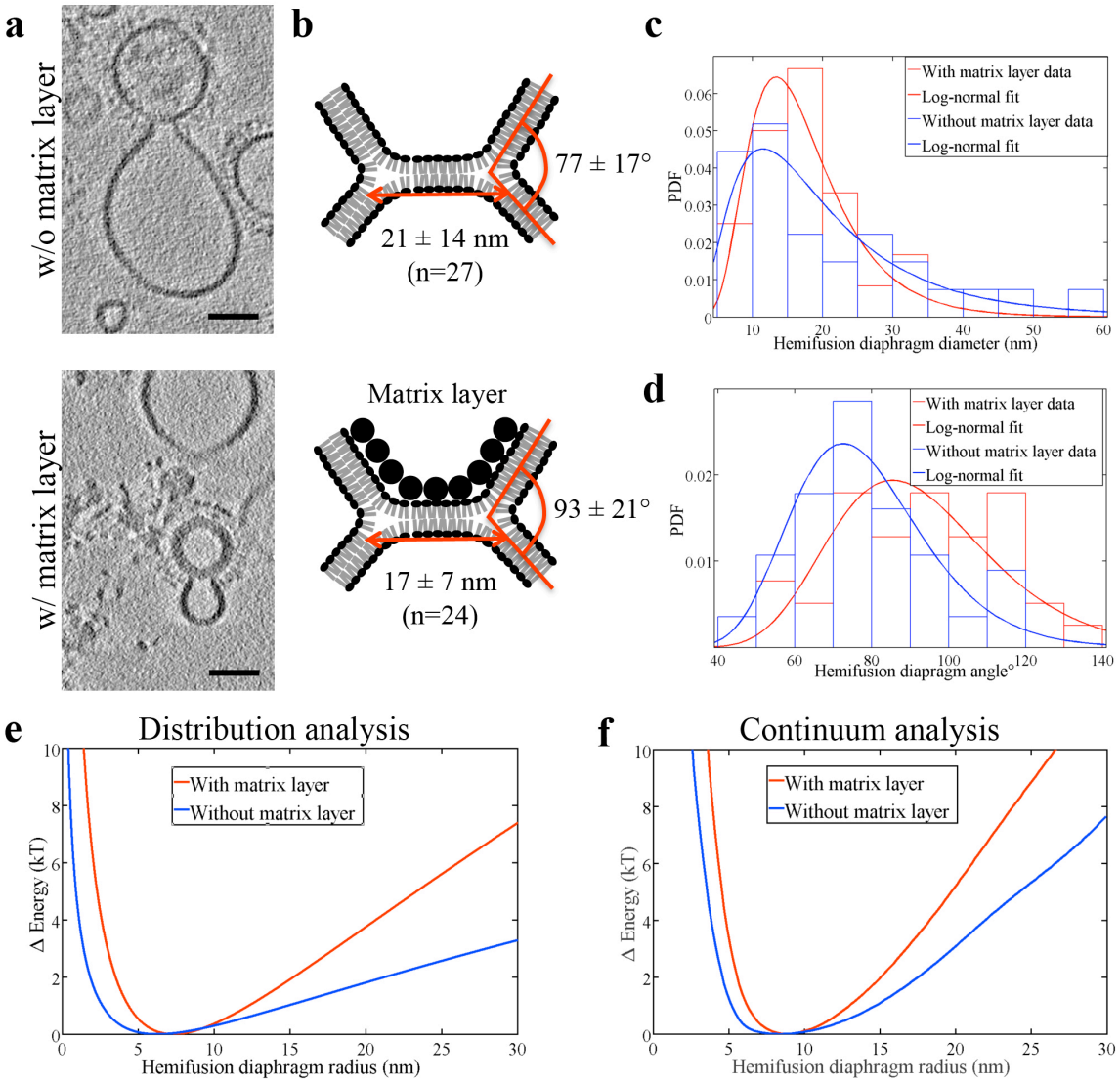

Supplementary Figure 4. Geometry of hemifusion diaphragm is modulated by presence of matrix layer. a, Tomographic slices (3 nm thick), calculated by the weighted back projection method, from a tilt series acquired at defocus -1 μm with VPP capturing HDs without (top panel) and with matrix layer (bottom panel). Scale bars: 50 nm. **b**, Average angle and diameter of the population with and without matrix layer are

shown in schemas. Angle represents a mean of angles measured on two sites of multiple HDs. Averages were calculated from both diameters measured on fully formed HDs and maximal chord lengths measured on the partial HDs. **c** and **d**, Histogram and HD diameter probability density function (PDF) (**c**) and angle (**d**) distributions with and without matrix layer. **e**, Free energy (ΔkT), relative to the most probable diameter (D_0) calculated using [–ln Probability(D)], for datasets with or without matrix layer based on the probability distribution of pooled datasets of WT and G1S as a function of HD size. **f**, Free energy (ΔkT) calculated using continuum mechanics for bending moduli of membrane and membrane with matrix layer.

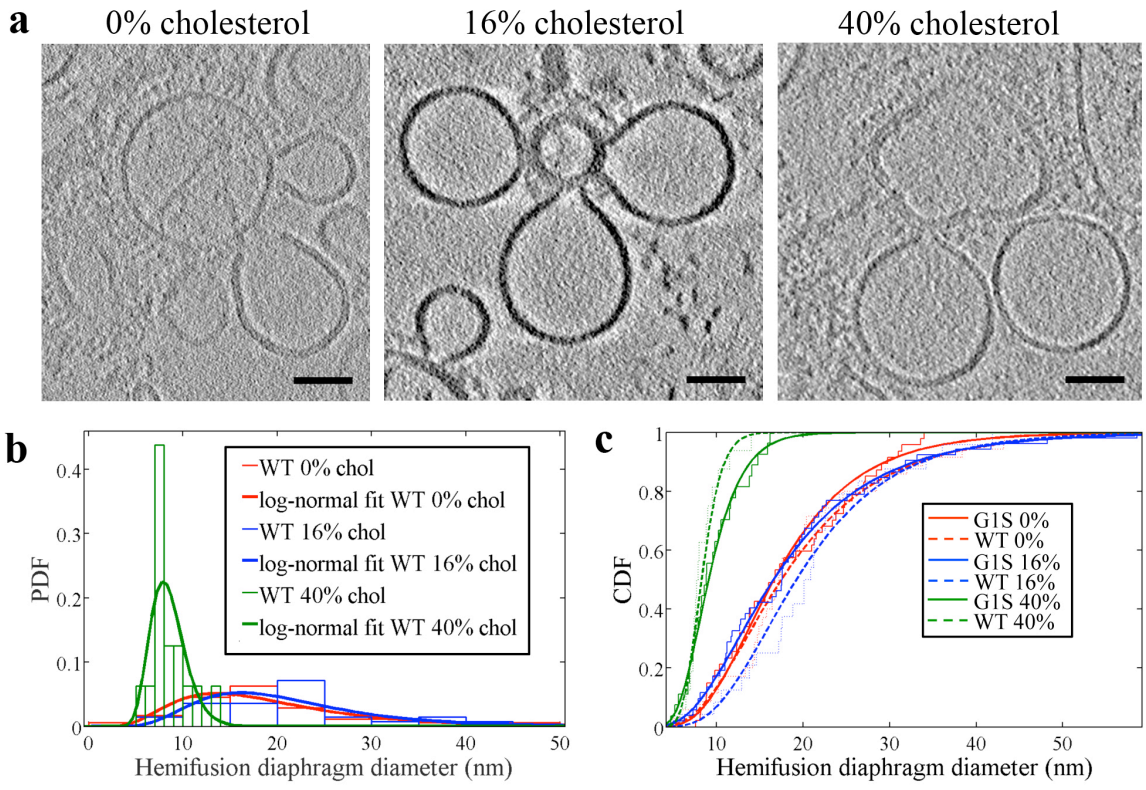

Supplementary Figure 5. WT HA forms HD with similar diameter as found in G1S HA mutant. WT VLP were mixed with liposomes containing either 0, 16 or 40 mol % cholesterol and incubated for 20 minutes at neutral pH and subsequently subjected to pH 5 at 37°C for approximately 2 minutes. **a**, 3 nm slices of a tomograms capturing WT VLP induced rupture (white arrow), lipid junction and HD at different cholesterol concentrations. Scale bar: 50 nm. **b**, Histograms and probability density functions (PDF) of the WT induced HD diameters at different cholesterol concentrations. **c**, Cumulative distribution functions (CDF) of HD diameter mediated by G1S VLP and WT VLP at different cholesterol concentrations. The fitting parameters and confidence bounds (95%) for the fits are summarized in Supplementary Table 2.

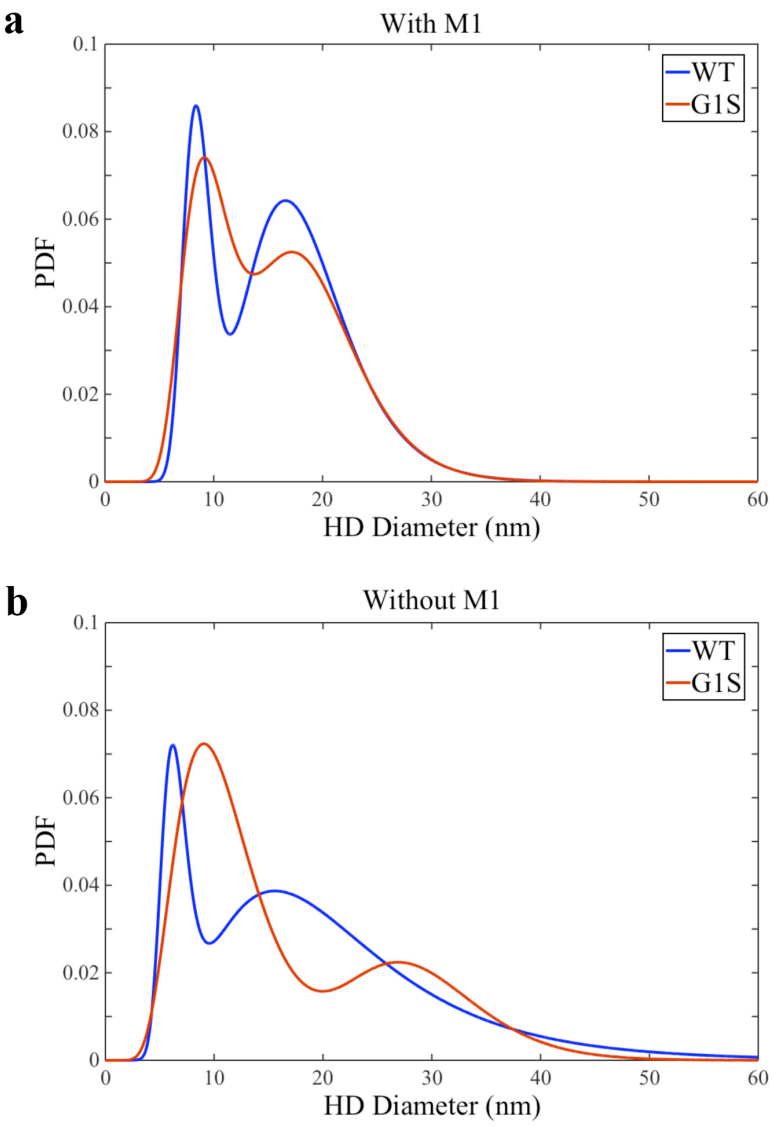

Supplementary Figure 6. WT and G1S combined distributions depend on the presence and absence of M1. The HD size distributions (CDFs) of WT and G1S (combining 0, 16 and 40 mol % cholesterol), with (**a**) and without M1 (**b**) were described by a sum of 2 lognormal distributions $p \cdot \text{logncdf}(x,\mu_1,\sigma_1) + (1-p) \cdot \text{logncdf}(x,\mu_2,\sigma_2)$. The resulting fitting parameters were used to produce the PDFs shown in the figure using the relationship: $p \cdot \text{lognpdf}(x,\mu_1,\sigma_1) + (1-p) \cdot \text{lognpdf}(x,\mu_2,\sigma_2)$. The fitting parameters and confidence bounds (95%) for the fits are summarized in Supplementary Table 2.

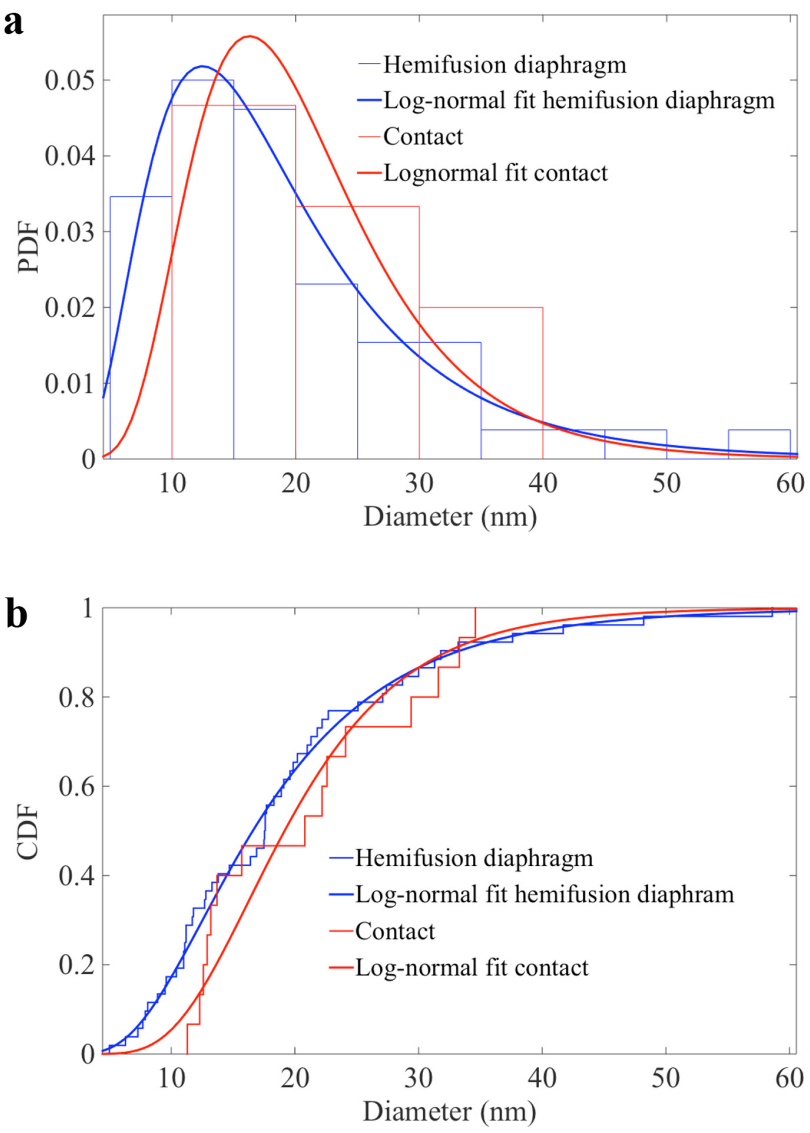

Supplementary Figure 7. Distribution of binding areas diameters is similar to the distribution of HD diameters for spherical G1S VLP showing one HD per liposome. **a**, Histograms with lognormally fit probability density functions (PDF) and **b**, cumulative distribution functions (CDF) of HD and binding area diameters mediated by G1S VLP. No significant difference between the two distributions was found. The maximum difference between the cumulative distributions, D, is: 0.3097 with a corresponding p value of: 0.111 (Kolmogorov-Smirnov test). The mean diameter of HD (G1S VLP) was

19±11 nm (n=51) and the mean diameter of binding area was 24±9 nm (n=19). The fitting parameters and confidence bounds (95%) for the fits are summarized in Supplementary Table 3.

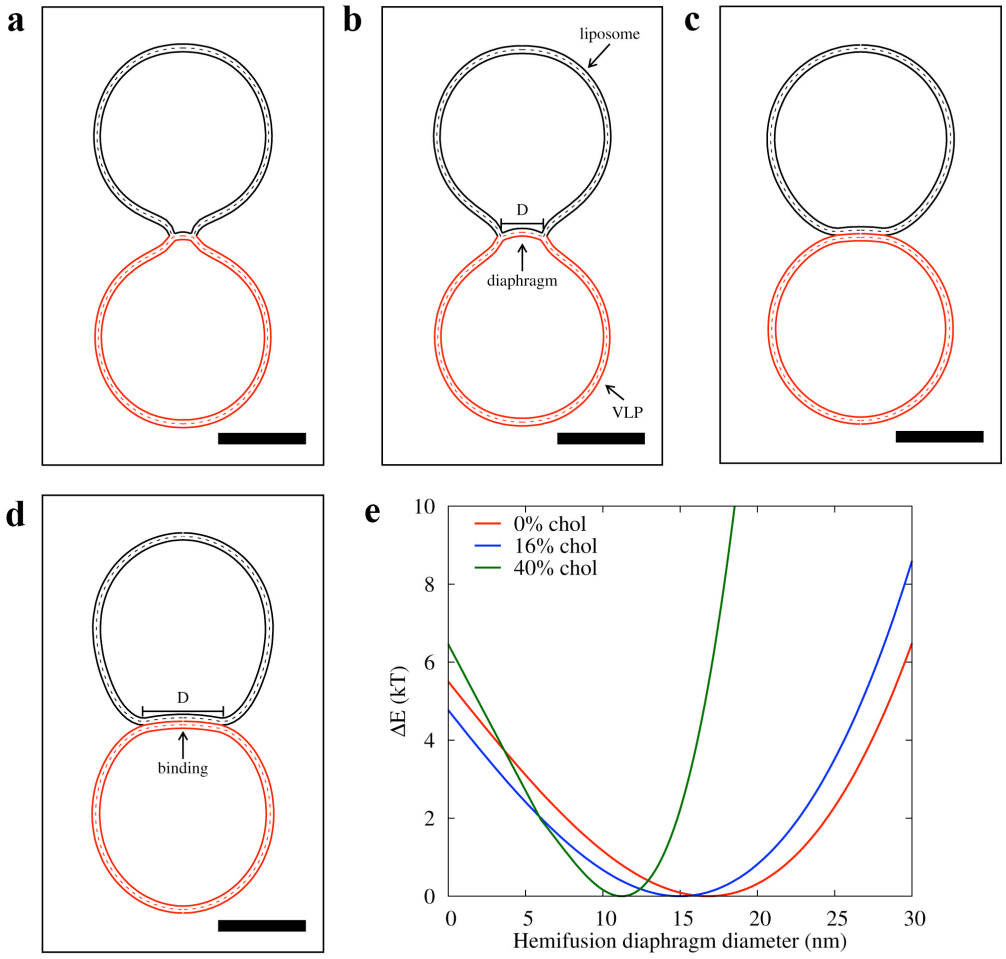

Supplementary Figure 8. Continuum analysis of hemifusion along the hemifusion stalk expansion pathway for a moderately sized HD. a, HD with diameter D = 10 nm and **b**, HD with a large diameter D = 24 nm. In order to evaluate Helfrich energy of HD growth under fixed conditions, the distal monolayer surface areas are conserved; the proximal monolayers are allowed to stretch/compress. The area of the distal monolayers (the inner black liposome curve and the inner red VLP curve respectively) in panels **a** and **b** are the same. The areas of the proximal monolayers (the outer black and red curves,

respectively) in panel **b** are smaller than in panel **a** resulting in an increase in energy of compression. **c** and **d**, Liposomes of different binding area prior to rupture and lipidic junction formation. Scale bars 50 nm. **e**, Change in Helfrich energy ΔE relative to the energy at the minimum HD diameter.

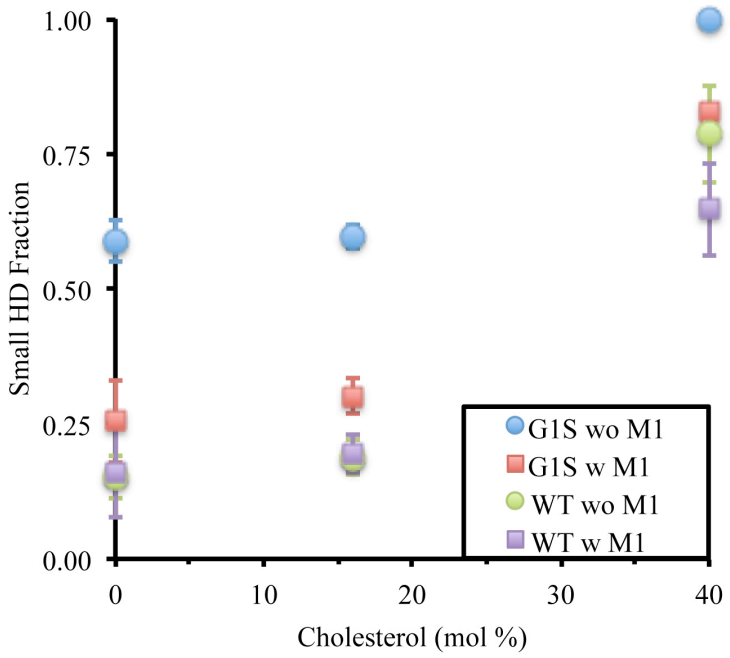

Supplementary Figure 9. Fractional contribution of the hemifusion stalk pathway as a function of cholesterol. Under the hypothesis that the distributional properties (mean and variance) of the two pathways described in Fig. S6 remains invariant with cholesterol and that only their relative fraction changes, each data set (G1S and WT as a function of cholesterol) was fit with only one free parameter – the fractional contribution of the hemi-fusion stalk pathway. The increase in the hemi-fusion stalk pathway occurring between 16 mol % and 40 mol % in both WT and G1S is in agreement with the continuum analysis dependence on cholesterol (Fig. 4f inset). The values represent the fractional contribution (+/- 95% confidence) obtained using a sum of two lognormal

distributions. The fractional fitting parameter and confidence bounds (95%) for the fits are summarized in Supplementary Table 4.

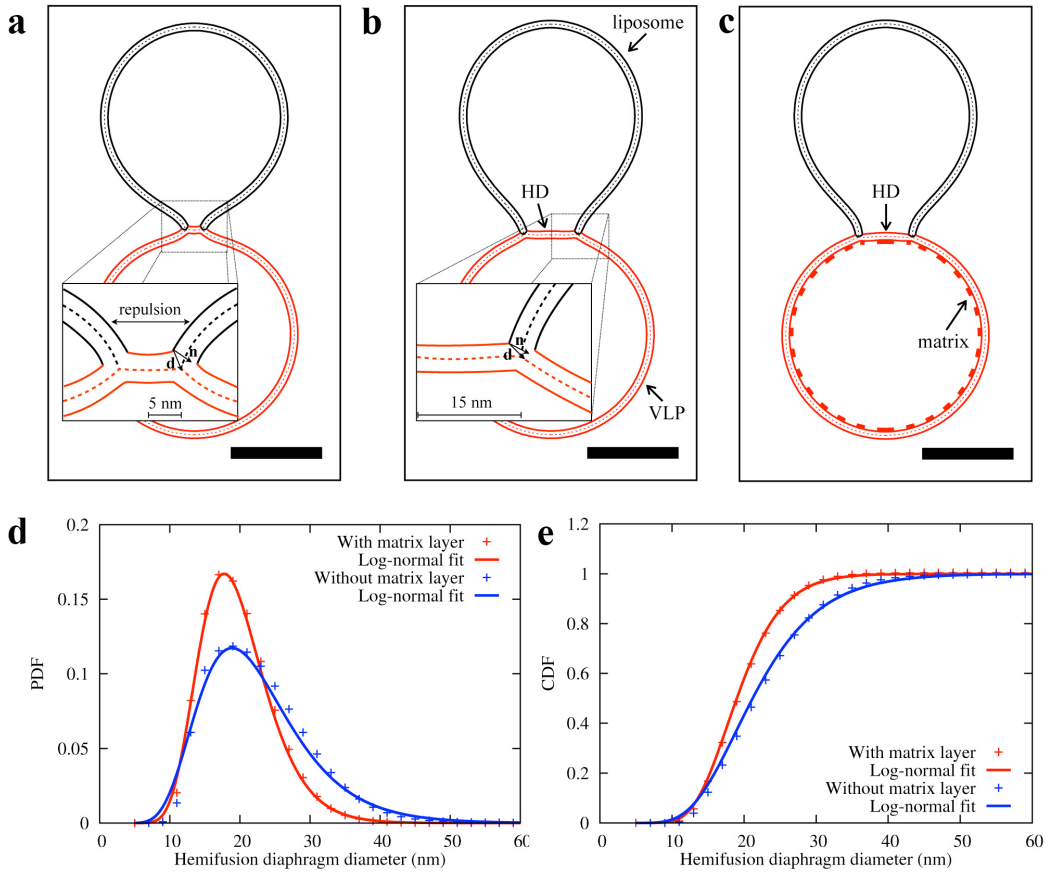

Supplementary Figure 10. Continuum analysis of hemifusion diaphragm in the presence and absence of matrix layer. Panels A-C show the cross-section of minimal energy shapes of the VLP-liposome merger product. The solid black curves are the liposomal neutral surface monolayers, the solid red curves are the VLP-HD neutral surface monolayers; the dashed curves are the mid-plane surfaces. The scale bar represents 50 nm. **a**, For small HD radii (5 nm), self-repulsion of the neck of the inner liposomal monolayer and a large tilt deformation of the "Y" (inset) widen the HD. **b**, For

large HD radii (15 nm) the neck of the liposome bilayer is less pinched but further HD expansion is prevented by the increasing energy of the "Y" junction. **c**, When the matrix layer is present (thick dashed red curve, HD radius 15 nm), HD curvature matches more closely the curvature of the VLP than when the matrix layer is absent (**b**). **d**, Compares the probability distribution function calculated using the continuum model (plusses) against the log-normal PDF distribution (solid curves) as a function of HD diameter D. The parameters are $\sigma = 0.26$ and $\mu = 2.25$ (red curves: with matrix layer, mean 9.83, variance 6.75) and for $\sigma = 0.34$ and $\mu = 2.36$ (blue curves: without matrix layer, mean 11.23, variance 15.46). **e**, Shows the cumulative distribution functions calculated using the continuum model and the lognormal CDF - for the same parameters.

SUPPLEMENTARY TABLES

Supplementary Table 1. Summary of average HD diameters and frequency of rupture of the liposomes

	Hemifusion diameter (nm)		
	0% cholesterol	16% cholesterol	40% cholesterol
WT	19.7±9.7	21.1±8.4	8.5±2.0
G1S	18.3±7.9	19.1±10.9	9.3±3.2

	Rupture (%)		
	0% cholesterol	16% cholesterol	40% cholesterol
WT	41% (n=51)	67% (n=18)	6% (n=16)
G1S	40% (n=64)	53% (n=34)	10% (n=29)

Cholesterol (mol %)	0	14	38-43
Elastic area compressibility modulus K (mN/m)	193±20	216±12	333±9 - 609±44

Liposome lipid composition	A	B	C
Cholesterol (mol %)	0	16	40
Estimated spontaneous monolayer curvature J (nm^{-1})	-0.0159	-0.12964	-0.24314

Supplementary Table 1. Summary of average HD diameters and frequency of rupture of the liposomes. Summary of average HD diameters and frequency of rupture at different cholesterol molar concentrations in the liposomes (top table). Middle table shows elastic area compressibility modulus K (mN/m) values for different cholesterol concentrations [5]. Bottom table shows estimated spontaneous monolayer curvatures J (nm^{-1}) for liposome lipid composition A, B and C (Material and Methods). J values were calculated based on molar concentration and J of individual lipids [6].

Supplementary Table 2. Log-normal fitting parameters for the curves presented in Fig. S6

	Mu1	Mu2	p	Sigma1	Sigma2	RMSE
G1S - M1	2.355 (2.328, 2.382)	3.357 (3.331, 3.384)	0.6909 (0.6621, 0.7197)	0.3901 (0.3634, 0.4167)	0.2085 (0.1772, 0.2397)	0.01282
WT - M1	1.846 (1.759, 1.934)	2.973 (2.92, 3.027)	0.1933 (0.1346, 0.2521)	0.1868 (0.08349, 0.2901)	0.4765 (0.4248, 0.5282)	0.02337
G1S + M1	2.267 (2.168, 2.367)	2.941 (2.873, 3.009)	0.4416 (0.3148, 0.5684)	0.2582 (0.1923, 0.3242)	0.2432 (0.1974, 0.289)	0.01627
WT + M1	2.143 (2.068, 2.217)	2.878 (2.833, 2.924)	0.2751 (0.1943, 0.356)	0.1552 (0.08031, 0.2301)	0.262 (0.2168, 0.3072)	0.02502

Supplementary Table 2. Log-normal fitting parameters for the curves presented in Fig. S6.

Supplementary Table 3. Log-normal fitting parameters for the curves presented in Fig. S7

	Mu (95% confidence interval)	Sigma (95% confidence interval)
WT 0 mol%	2.86 (2.69 3.03)	0.51 (0.39 0.63)
WT 16 mol%	2.98 (2.82 3.14)	0.43 (0.31 0.55)
WT 40 mol%	2.11 (2.00 2.22)	0.22 (0.14 0.30)
G1S 0 mol%	2.81 (2.68 2.94)	0.45 (0.36 0.54)
G1S 16 mol%	2.81 (2.66 2.95)	0.54 (0.43 0.64)
G1S 40 mol%	2.21 (2.08 2.34)	0.33 (0.24 0.42)
Contact (binding zone)	3.08 (2.88 3.27)	0.44 (0.29 0.58)
Hemifusion (G1S 16 mol%)	2.81 (2.66 2.95)	0.54 (0.43 0.64)

Supplementary Table 3. Log-normal fitting parameters for the curves presented in Fig. S7.

Supplementary Table 4. Fractional fitting parameters and confidence bounds (95%) for the data presented in Fig. S9

G1S	Cholesterol (%)	Small HD Fraction	-95%	95%
w/o M1	0	0.59	0.55	0.63
w/o M1	16	0.60	0.57	0.62
w/o M1	40	1.00		
w M1	0	0.26	0.18	0.33
w M1	16	0.30	0.27	0.33
w M1	40	0.83	0.78	0.88
WT				
w/o M1	0	0.15	0.11	0.19
w/o M1	16	0.19	0.16	0.22
w/o M1	40	0.79	0.70	0.88
w M1	0	0.16	0.08	0.25
w M1	16	0.19	0.16	0.23
w M1	40	0.65	0.56	0.73

Supplementary Table 4. Fractional fitting parameters and confidence bounds (95%) for the data presented in Fig. S9.

SUPPLEMENTARY VIDEOS

Supplementary Video 1

Video of tomogram shows "Y" (lipidic) junctions mediated by G1S VLP corresponding to Fig. 2b. Tomogram was acquired at defocus -5µm without VPP and denoised using nonlinear anisotropic diffusion (NAD) filter [7] with k value 10, and 10 iterations. Scale bar: 50 nm

Supplementary Video 2

Video of tomogram shows "Y" (lipidic) junctions mediated by G1S VLP corresponding to Fig. 2c. Tomogram was acquired at defocus -1µm with VPP and denoised using NAD filter with k value 10 and 10 iterations. Scale bar: 50 nm

Supplementary Video 3

Video of tomogram shows liposome and complete HD connected to the membrane of the G1S filamentous VLP from top (corresponding to Fig. 2e). Tomogram was acquired at defocus -1µm with VPP.

Supplementary Video 4

Animated visualization of isosurface of spherical VLP and several liposomes at low pH shown in Fig. 2c and 3a-d. Liposome marked by A corresponds to the liposome in Fig. 2c and 3a. Liposome marked by C corresponds to the liposome in Fig. 3c. Lipidic junctions are marked by red arrowhead in the first frame of the video.

Supplementary Video 5

Video of tomogram shows ruptured liposomes and lipidic junctions with G1S filamentous VLP (corresponding to Fig. 3e). Tomogram was acquired at defocus -1µm with VPP and denoised using the NAD filter with a k value of 1, for 10 iterations.

Supplementary Video 6

Animated visualization of isosurface of ruptured liposomes and lipidic junctions with G1S filamentous VLP (corresponding to Fig. 3e). Scale bar: 50 nm

Supplementary Video 7

Video of tomogram shows WT VLP and liposomes fusion product (FP) after complete fusion characteristic of areas of membrane free of influenza glycoproteins. Red arrows and marks sparsely distributed influenza glycoproteins and red line highlights the membrane harboring influenza glycoproteins. The unmarked area is free of influenza glycoproteins. Scale bar: 50 nm.

SUPPLEMENTARY REFERENCES

1 Zhelev, D. V., Stoicheva, N., Scherrer, P. & Needham, D. Interaction of synthetic HA2 influenza fusion peptide analog with model membranes. *Biophysical journal* **81**, 285-304, doi:10.1016/S0006-3495(01)75699-8 (2001).

2 Nagle, J. F. & Tristram-Nagle, S. Structure of lipid bilayers. *Biochim Biophys Acta* **1469**, 159-195 (2000).

3 Hamm, M. & Kozlov, M. M. Elastic energy of tilt and bending of fluid membranes. *Eur. Phys. J.* **3**, 323-335 (2000).

4 Aeffner, S., Reusch, T., Weinhausen, B. & Salditt, T. Energetics of stalk intermediates in membrane fusion are controlled by lipid composition. *Proceedings of the National Academy of Sciences of the United States of America* **109**, E1609-1618, doi:10.1073/pnas.1119442109 (2012).

5 Needham, D. & Nunn, R. S. Elastic deformation and failure of lipid bilayer membranes containing cholesterol. *Biophysical journal* **58**, 997-1009, doi:10.1016/S0006-3495(90)82444-9 (1990).

6 Kollmitzer, B., Heftberger, P., Rappolt, M. & Pabst, G. Monolayer spontaneous curvature of raft-forming membrane lipids. *Soft Matter* **9**, 10877-10884, doi:10.1039/C3SM51829A (2013).

7 Frangakis, A. S. & Hegerl, R. Noise reduction in electron tomographic reconstructions using nonlinear anisotropic diffusion. *J Struct Biol* **135**, 239-250, doi:10.1006/jsbi.2001.4406 (2001).